Ultrasonic study of the temperature and pressure dependences of the elastic properties of fcc Co-Mn alloy single crystals

G. A. Saunders, D. Ball,* M. Cankurtaran,† and Q. Wang
School of Physics, University of Bath, Bath BA2 7AY, United Kingdom

E. Arnscheidt, C. Jacobs, F. Imbierwitz, and J. Pelzl
Arbeitsgruppe Festkörperspekttroscopie, Institut für Experimentalphysik, Ruhr-Universität Bochum, D-44780 Bochum, Germany

H. Bach
Kristall-laboratory, Institut für Experimentalphysik, Ruhr-Universität Bochum, D-44780 Bochum, Germany
(Received 7 August 1996; revised manuscript received 13 January 1997)

To search for ramifications of magnetovolume effects in the magnetoelasticity of Co-Mn alloys, the elastic and nonlinear acoustic properties of single crystals with compositions $Co_{75}Mn_{25}$, $Co_{68}Mn_{32}$, $Co_{52}Mn_{48}$, and $Co_{46}Mn_{54}$, which have different magnetic configurations, have been determined ultrasonically. Pulse-echo-overlap measurements of the velocities of ultrasonic modes have been used to determine the three independent elastic-stiffness tensor components C_{IJ} and the adiabatic bulk modulus B^S, as a function of temperature in the range from 4.2 up to about 800 K, and the pressure derivatives $(\partial C_{IJ}/\partial P)_{P=0}$ and $(\partial B^S/\partial P)_{P=0}$ at room temperature. These measurements of the elastic and nonlinear acoustic behavior of fcc Co-Mn alloys assist understanding of the structural and magnetic phase stability in this alloy system. Two of the alloys studied ($Co_{52}Mn_{48}$ and $Co_{46}Mn_{54}$) are antiferromagnetic at room temperature; their elastic-stiffness tensor components and bulk moduli are affected by the onset of antiferromagnetic ordering and strong magnetoelastic coupling in the antiferromagnetic phase. The $Co_{68}Mn_{32}$ alloy, with composition centered between the superantiferromagnetic and superparamagnetic regions in the phase diagram, does not undergo any transition. The temperature dependences of the elastic stiffnesses associated with the three independent ultrasonic modes propagated in the austenite and martensite phases of the ferromagnetic $Co_{75}Mn_{25}$ alloy show that the $\epsilon \rightarrow \gamma$ transition is strongly first order; the absence of long-wavelength acoustic-mode softening shows that its driving mechanism is not elastic in origin. Application of pressure does not induce acoustic mode softening for any of these alloys: the pressure derivatives $(\partial C_{IJ}/\partial P)_{P=0}$ and $(\partial B^S/\partial P)_{P=0}$ are positive. The long-wavelength longitudinal-acoustic-mode Grüneisen parameters of antiferromagnetic $Co_{46}Mn_{54}$ show the unusual feature of being smaller than those for the shear waves: magnetovolume contributions to vibrational anharmonicity are stronger for longitudinal than for shear waves. The longitudinal-mode gamma $\gamma_{L[110]}$ of this $Co_{46}Mn_{54}$ alloy passes through a maximum value of 7.0 at 388 K: the vibrational anharmonicity of this mode is markedly enhanced in the vicinity of the Néel temperature. [S0163-1829(97)06017-7]

I. INTRODUCTION

Transition-metal elements and alloys with the fcc structure can show instabilities of their magnetic moments with respect to atomic volume.[1–4] Structural martensitic transitions, and also Invar behavior, in magnetic $3d$ alloys are driven by magnetovolume effects originating in magnetoelastic interactions. As the electron concentration per atom (e/a ratio) alters across the Co-Mn binary-system, these alloys show a complex pattern of intriguing structural and magnetic phase stabilities.[5,6] The parent elements are themselves multiphase. At 417 ± 10 K ferromagnetic cobalt undergoes a martensitic phase transition from the hcp ϵ phase, stable at room temperature, to the fcc γ allotropic form, which is then retained up to the melting point. Manganese has four different phases; the fcc γ allotrope has a very limited range (1373–1411 K) of phase stability, which can be enhanced by alloying with a neighboring element such as cobalt. γ Mn is a type-I antiferromagnet; the fcc lattice is frustrated: it is not possible for every atomic spin to have a nearest neighbor with an opposing spin, and theoretical aspects are interesting because the magnetism may be noncollinear. Competing ferromagnetic (FM) and antiferromagnetic (AFM) interactions are one of the more fascinating features of the binary Co-Mn alloys. A magnetic phase diagram has been compiled from magnetic and neutron diffraction studies on polycrystalline samples;[5] in a simplified version the $\epsilon \rightarrow \gamma$ and $\gamma \rightarrow \epsilon$ transitions are represented by single boundaries.[6] Alloys containing up to about 25 at. % Mn are ferromagnetic,[7] while above about 43 at. % Mn they are antiferromagnetic.[8] These magnetic alloys can show large magnetovolume effects and Invar behavior.[2,9,10] Co-rich alloys in the $Co_{100-x}Mn_x$ system with $x < 25$ at. % show the fcc (γ) to hcp (ε) martensitic transition. However, the onset of long-range AFM order at $x > 32$ at.% causes a large increase in the atomic volume. Thermal expansion measurements have shown that there are positive magnetovolume effects in both the FM and AFM ground states.[11] For alloys with $25 < x < 43$ at. % the phase diagram indicates a paramagnetic (PM) state with possibilities of superparamagnetism or superantiferromagnetism for compositions close to the FM and AFM regions, respectively.[5] It may be useful to

recall that the concept of superantiferromagnetism was introduced by Néel[12] to describe the magnetic behavior of an ensemble of finely dispersed antiferromagnetic NiO particles; its present status can be assessed from a review of fine particle magnetic oxides.[13] The existence of superantiferromagnetism in fcc Co-Mn alloys in the composition range 33–52 at. % Mn has been attested to in magnetic neutron diffraction studies.[14]

Anomalies found previously[15] in the temperature dependences of the elastic stiffnesses of an AFM $Co_{46}Mn_{54}$ alloy in the vicinity of the Néel temperature (T_N) have indicated strong magnetoelastic coupling in this alloy, which shows Invar anomalies in the thermal expansion. The observation that magnetovolume instabilities and magnetoelastic interactions have important ramifications in the elastic properties of $Co_{46}Mn_{54}$ prompted a more comprehensive ultrasonic study of the elastic and nonlinear acoustic behavior of other monocrystalline alloys in this binary system. In addition to examining fundamental elastic behavior, ultrasonic wave velocity measurements provide a powerful tool for study of magnetic or structural phase relationships. In an AFM or FM crystal there is a contribution to the total energy arising from the interatomic magnetic interactions between the aligned magnetic moments. Since the elastic-stiffness tensor components C_{IJ} are directly related to the second derivatives of the free energy with respect to strain, they include an intrinsic contribution due to magnetic ordering. The hydrostatic-pressure derivatives $(\partial C_{IJ}/\partial P)_{P=0}$ of the elastic-stiffness moduli are related to the third derivatives of the free energy with respect to strain, and hence to the vibrational anharmonicity of the long-wavelength acoustic phonons, and so must also include magnetoelastic contributions. To provide information needed to develop an understanding of the structural and magnetic phase stabilities in the Co-Mn alloys and in Co itself, the alloys investigated include one in the FM composition range, which undergoes $\varepsilon \rightarrow \gamma$ and $\gamma \rightarrow \varepsilon$ transitions, and others in the AFM and PM regions of the phase diagram. To examine experimentally how the development of antiferromagnetic ordering influences the vibrational anharmonicity of acoustic phonons, a little known aspect of magnetoelasticity, the effects of pressure on the velocity of longitudinal ultrasonic waves propagated in $Co_{46}Mn_{54}$ have been measured as a function of temperature up into the vicinity of T_N.

II. EXPERIMENTAL PROCEDURE

Co-Mn alloy single crystals, with compositions given in Table I(a), were grown from high-purity elements by a modified Bridgman-Stockbarger process. Inspection of the phase diagram[5,6] reveals that the $Co_{75}Mn_{25}$ alloy comes in the FM phase region and can be expected to undergo $\varepsilon \rightarrow \gamma$ and the reverse $\gamma \rightarrow \varepsilon$ transitions, when its temperature is altered. The paramagnetic $Co_{68}Mn_{32}$ alloy has a composition near the center of the region of the phase diagram between the superantiferromagnetic (SAF) and superparamagnetic (SP) forms. The $Co_{52}Mn_{48}$ and $Co_{46}Mn_{54}$ alloys are in the AFM phase at room temperature. Crystal quality was examined by taking Laue back-reflection photographs along the boule. Microprobe analysis scans around the crystal showed their compositions were within ± 1 at. % of their stated concentrations. The crystals were orientated to $\pm 0.5°$ on a three-arc goniometer using Laue back-reflection photography. Samples, large enough for precision measurements of ultrasonic wave velocities, were cut and polished to have two faces, normal to the [110] crystallographic axis, flat to surface irregularities of about 3 μm and parallel to better than 10^{-3} rad. After completion of the [110] mode experiments, the $Co_{68}Mn_{32}$, $Co_{52}Mn_{48}$, and $Co_{46}Mn_{54}$ alloys crystals were recut along the [001] crystallographic axis to enable measurements to be made at room temperature of C_{11}, C_{44}, $(\partial C_{11}/\partial P)_{P=0}$, and $(\partial C_{44}/\partial P)_{P=0}$, to check internal consistency of the results.

To generate and detect ultrasonic pulses, X- or Y-cut (for longitudinal and shear waves, respectively) 10-MHz quartz transducers were bonded to the specimen using Apiezon N for low-temperature experiments; Krautkrämer ZGM high-temperature coupling paste was employed to make measurements above room temperature. Dow resin was used as bonding material for high-pressure experiments. Ultrasonic pulse transit times were measured using a pulse-echo-overlap system,[16] capable of resolution of velocity changes to 1 part in 10^5 and particularly well suited to determination of pressure or temperature-induced changes in velocity. The temperature dependence of ultrasound velocity was measured between 4.2 and 800 K. The dependence of ultrasonic wave velocity upon hydrostatic pressure was measured at room temperature for the longitudinal and both shear wave modes propagated in $\langle 110 \rangle$ and $\langle 001 \rangle$ directions in the alloys and up to 423 K for the longitudinal mode propagated in $\langle 110 \rangle$ direction in $Co_{46}Mn_{54}$. Hydrostatic pressure up to 0.16 GPa was applied in a piston-and-cylinder apparatus using silicone oil as the pressure-transmitting medium. Pressure was measured using a precalibrated manganin resistance gauge. Pressure-induced changes in the sample dimensions were accounted for by using the ''natural velocity (W)'' techniques.[17,18]

III. THE ELASTIC STIFFNESS TENSOR COMPONENTS OF Co-Mn ALLOYS

The velocities of the three ultrasonic modes, propagated along the [110] direction, and the sample density have been used to determine the elastic stiffnesses $C_L(=(C_{11}+C_{12}+2C_{44})/2)$, $C'(=(C_{11}-C_{12})/2)$, and C_{44}. The results, together with those of C_{11} and C_{44}, obtained from the longitudinal and shear modes propagated along the [001] direction, and the bulk modulus $B^S(=(C_{11}+2C_{12})/3)$, at room temperature are given in Table I(a). The elastic compliance tensor components S_{IJ}^S, and the linear K_{11}^S and volume K^S compressibilities of Co-Mn alloys at room temperature are given in Table II. Like those of other AFM Invar alloys, whose elastic-stiffness tensor components are compiled in Table I(b), the volume-dependent elastic stiffnesses C_{11} and C_L and the bulk modulus B^S of Co-Mn alloys are small in comparison with those of the parent $3d$ transition metals and Ni, Fe [Table I(b)] and hcp Co ($C_{11}=306$ GPa, $C_{33}=357$ GPa, $C_{12}=165$ GPa, $C_{13}=102$ GPa, $C'=71$ GPa, $C_{44}=75$ GPa and $B^S=190$ GPa[25]).

In general, Invar anomalies are observed for $3d$ transition-metal FM alloys having an e/a ratio of about 8.5 and AFM alloys with e/a about 7.5.[2,10] When the e/a ratio comes into the AFM and FM Invar regimes, the values of the

TABLE I. (a) Elastic stiffness tensor components C_{IJ}, adiabatic bulk modulus B^S, lattice parameter, density, e/a ratio, and shear anisotropy ratio A of fcc Co-Mn alloys. (b) Elastic stiffness tensor components C_{IJ}, bulk modulus B^S, e/a ratio, and shear anisotropy ratio A of transition-metal elements and alloys at room temperature.

(a)

C_{IJ} (GPa)	$Co_{75}Mn_{25}$ (293 K) FM, austenite phase	$Co_{68}Mn_{32}$ (293 K) PM		$Co_{52}Mn_{48}$ (291 K) AFM		$Co_{46}Mn_{54}$ (298 K) AFM	
		[110] mode	[001] mode	[110] mode	[001] mode	[110] mode	[001] mode
C_{11}	184.4±1.4	198.6 ± 3.4	197.8±1.0	178.4 ± 3.2	177.3±1.0	158.0 ± 3.0	158.7±1.0
C_{44}	137.4±0.7	141.9 ± 2.8	143.6±2.8	124.6 ± 2.6	126.8±2.8	130.2 ± 2.1	129.6±2.8
C_{12}	99.8±1.3	100.3 ± 3.7		91.6 ± 3.5		81.4 ± 3.3	
C'	42.3±0.3	49.1 ± 0.8		43.4 ± 0.7		38.3 ± 0.6	
C_L	279.5±1.0	291.3 ± 4.1		259.0 ± 5.1		249.9 ± 4.2	
B^S	128.0±1.3	133.1±2.0		120.5±2.1		107.0±1.9	
lattice parameter	0.3575	0.3584		0.3606		0.3626	
density (kg m^{-3})	8470	8362		7970		7870	
e/a	8.5	8.36		8.04		7.92	
A	3.25	2.89		2.74		3.4	

(b)

C_{IJ} (GPa)	Ni	Fe	$Fe_{60}Mn_{40}$ (293 K) AFM	$Mn_{73}Ni_{27}$ (293 K) AFM	$Mn_{80.5}Ni_{19.5}$ (293 K) AFM	$Mn_{78}Pt_{22}$ (293 K) AFM	$Co_{68}Ni_{32}$ (295 K) FM	$Fe_{72}Pt_{28}$ (290 K) FM
Ref.	19	19	20	21	21	22	23	24
C_{11}	247	230	170±1	129	113	94.2±0.1	238.7	143.9
C_{12}	153	136	98±2	77	48	35.8±0.1	155.3	107
C_{44}	122	117	141±1	98	110	84.7±0.3	131.5	80
C'	47	47	36±1	26	32	29.2±0.1	41.7	18.2
C_L	322	309	275±5	201	191	149.7	328.5	205.5
B^S	184	167	123±2	94	70	55.2±0.3	183.1	120
e/a	10	8	7.60	7.81	7.58	7.66	9.32	8.56
A	2.60	2.49	3.92	3.77	3.44	2.90	3.15	4.40

elastic moduli tend to be comparatively small.[20–22] Lenkkeri[26] has noted systematic trends with electron concentration for the elastic stiffnesses of fcc alloys of $3d$ transition metals in the range from γ Mn ($e/a=7$) to Cu ($e/a=11$). The bulk modulus B^S and the shear elastic stiffnesses C' and C_{44} of the Co-Mn alloys conform with these trends. Furthermore for the AFM and FM Co-Mn alloys the tensor component C_{11} is small compared with those of the parent elements; this is also true for C_L, which corresponds to a longitudinal wave propagated along a $\langle 110 \rangle$ direction [Table I(a)]. This implies that long-wavelength longitudinal acoustic phonons are relatively soft. Another instructive observation is that the longitudinal elastic stiffnesses C_{11} and C_L and the bulk modulus B^S of the fcc Co-Mn alloys are also small compared with those of the FM fcc $Co_{68}Ni_{32}$ alloy [Table I(b)]. Total-energy band calculations[3,27] for FM alloys, using a fixed-spin-moment (FSM) procedure, have established that the energy-volume curve has a low-spin (LS) minimum centered at low volume and a high-spin (HS) minimum at high volume. For FM Invar alloys the HS solution defines the

ground state at low temperatures and the LS solution defines the ground state at high temperatures. The energy difference $\Delta E(=E_{\mathrm{LS}}-E_{\mathrm{HS}})$ between the minima of the LS and HS branches is large and positive for an alloy with an e/a ratio greater than 9. Hence such an alloy shows either no, or small, magnetovolume effects. The $Co_{68}Ni_{32}$ alloy has an e/a ratio of 9.32, outside the range for the FM Invars, and in consequence is a stable fcc ferromagnet.[10] Therefore, the elastic-stiffness tensor components and the bulk modulus of the $Co_{68}Ni_{52}$ alloy [Table I(b)] are comparable with those of transition-element metals—substantially larger than those of the Co-Mn alloys [Table I(a)].

The theoretical explanation of the source of the Invar behavior in FM alloys can be extended to AFM alloys with the proviso that such systems must be characterized by AFM and nonmagnetic (NM) states and that the FM HS state is replaced by an AFM HS state which, at low temperatures, has a minimum at a lower energy than the NM state.[3,27] The reduction of the longitudinal-mode stiffness in the AFM state of $Co_{46}Mn_{54}$ due to the magnetoelastic interaction leads in turn to a bulk modulus $B^S(=107\ \mathrm{GPa})$ which is much smaller than those of hcp Co [$B^S=190$ GPa (Ref. 25)] and fcc $Co_{68}Ni_{32}$ alloy [$B^S=183$ GPa (Ref. 23)]. Longitudinal-mode softening due to the magnetovolume interaction, which results in a small value for C_{11}, can be instrumental in reducing $(C_{11}-C_{12})/2$ in turn—as it does in γ Mn-Ni (Ref. 21) and $Mn_{76}Pt_{22}$ (Ref. 22) alloys. Due to the small value of the shear modulus $(C_{11}-C_{12})/2$, those Mn alloys [Table I(b)] and the Co-Mn alloys [Table I(a)] have a large value of the shear anisotropy ratio $A(=C_{44}/C')$. Small shear-mode stiffness enhanced by softening can be instrumental both in enabling martensitic phase transformation and in promoting Invar behavior in transition-metal alloys. We will consider whether this happens in the Co-Mn alloys in the next section.

IV. THE TEMPERATURE DEPENDENCES OF THE ULTRASONIC WAVE VELOCITIES AND ELASTIC-STIFFNESS TENSOR COMPONENTS OF Co-Mn ALLOY

The elastic stiffnesses C_L, C_{44}, and C' and the bulk modulus B^S of the $Co_{68}Mn_{32}$ single-crystal alloy increase smoothly with decreasing temperature and show an approximately linear temperature dependence over a wide range of temperatures from 700 down to about 100 K, and approach 0 K with a zero slope (Fig. 1). In the absence of instability due to an incipient phase change, such an increase in elastic stiffness with decreasing temperature is generally expected as a consequence of the vibrational anharmonicity. This alloy has the composition at which the superparamagnetic and superantiferromagnetic phase lines intersect at low temperatures in the magnetic phase diagram;[5] however, there are no indications that it shows effects which might correspond to such transitions in the temperature range of the experiments (Fig. 1). Hence, $Co_{68}Mn_{32}$ can be thought of as a reference material in assessment of the elastic properties of the paramagnetic state of Co-Mn alloys.

The behavior with temperature of the elastic-stiffness tensor components of the alloy of composition $Co_{46}Mn_{54}$, also shown in Fig. 1, has been interpreted in some detail previously.[15] Ultrasonic velocity measurements made for the

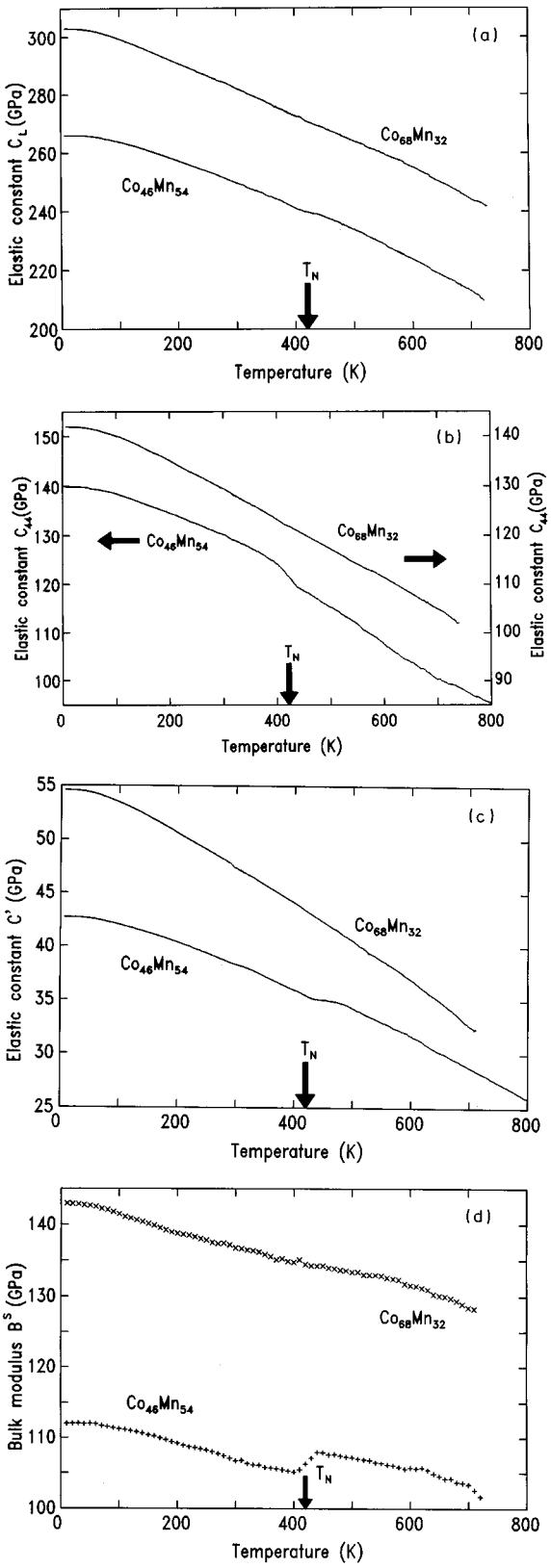

FIG. 1. The temperature dependences of the elastic-stiffnesses (a) C_L, (b) C_{44}, (c) $C'=(C_{11}-C_{12})/2$, and (d) the adiabatic bulk modulus B^S for the $Co_{46}Mn_{54}$ and $Co_{68}Mn_{32}$ alloys. The pulse-echo-overlap method (Ref. 16) used to make these measurements is capable of resolution of velocity changes to 1 part in 10^5: the structure of the velocity-temperature dependence is reliable, while the absolute error corresponds to that quoted in Table I(a).

TABLE II. The elastic compliance tensor components S_{IJ}^S and the linear K_{11}^S and volume K^S compressibilities of Co-Mn alloys at room temperature.

Elastic compliances (10^{-11} Pa^{-1})	$Co_{75}Mn_{25}$ (293 K) austenite phase	$Co_{68}Mn_{32}$ (293 K)	$Co_{52}Mn_{48}$ (291 K)	$Co_{46}Mn_{54}$ (298 K)
S_{11}^S	0.875±0.006	0.762±0.019	0.860±0.019	0.974±0.019
S_{12}^S	−0.307±0.004	−0.256±0.007	−0.292±0.007	−0.331±0.007
S_{44}^S	0.728±0.004	0.705±0.015	0.802±0.015	0.768±0.015
K_{11}^S (10^{-1} Pa^{-1})	0.260±0.006	0.250±0.006	0.277±0.006	0.312±0.006
K^S (10^{-11} Pa^{-1})	0.781±0.019	0.751±0.019	0.830±0.019	0.936±0.019

$Co_{52}Mn_{48}$ alloy, which also undergoes a paramagnetic to AFM transition, show rather similar, but not so well pronounced features as those observed for $Co_{46}Mn_{54}$. In the vicinity of the Néel temperature, estimated for $Co_{46}Mn_{54}$ from the anomaly in the elastic stiffnesses as 425 K, all the elastic-stiffness tensor components are affected by the onset of antiferromagnetic ordering and strong magnetoelastic coupling: there is a reduction in the elastic stiffnesses C_L and $(C_{11}-C_{12})/2$; in the case of C_{44} there is a change of slope to a higher value [see Figs. 1(a) to 1(c) and Table II]. A phenomenological interpretation of the elastic behavior with temperature was obtained on the basis of the Landau theory of second-order phase transitions.[15] Reduction of the bulk modulus in the AFM state [Fig. 1(d)], a feature in common with FM Invars, occurs because of the appearance of a spontaneous volume strain. The temperature dependences of the shear elastic stiffnesses result from a nonlinear coupling between the strain and the order parameter and are not a property of the Invar state but are determined by the exchange and magnetoelastic interactions in the magnetically ordered AFM state.

All the Co-Mn alloys studied have small values of the shear stiffness $(C_{11}-C_{12})/2$ [Table I(a)], a characteristic feature of fcc metals and alloys [Table I(b)]. The moment-volume instability, which is responsible for much of the anomalous thermal and acoustic behavior in $3d$ alloys,[9,10] is not strong enough to induce incipient martensitic transition in AFM $Co_{46}Mn_{54}$. However, the $\varepsilon\rightarrow\gamma$ and $\gamma\rightarrow\varepsilon$ transitions are characteristic of $Co_{100-x}Mn_x$ alloys containing less than about 32 at. % Mn.[5] Ultrasonic velocity measurements made as a function of temperature (or pressure) can provide valuable, in some cases definitive, information about the driving mechanism of transitions, in particular if they are displacive in type. The temperature dependences of the three independent elastic stiffnesses associated with ultrasonic waves propagated along a $\langle 110\rangle$ direction in the austenite γ-phase $Co_{75}Mn_{25}$ single-crystal alloy show clearly the effects of sound wave interactions and their relation to the transitions in this material (Fig. 2). The elastic stiffness C_L increases approximately linearly with decreasing temperature from 820 down to about 640 K. The Curie temperature is seen as a sharp change in slope at about 634 K; this may be compared with a value of 600 K deduced from the phase diagram given in Ref. 5. On warming up from 4.2 K the start temperature for the $\varepsilon\rightarrow\gamma$ transition is at about 436 K and the completion temperature is at 528 K. On cooling the $\gamma\rightarrow\varepsilon$ transition commences at 272 K. These martensitic transition temperatures differ substantially from those given in the phase diagram (which collates data obtained only on polycrystalline materials). The marked hysteresis effect shows that the $\varepsilon\rightarrow\gamma$ transition is strongly first order. The hysteresis effect is essentially absent in the temperature range above about 530 K. The temperature dependence of the shear stiffness C_{44} shows quite similar features [Fig. 2(b)].

One possible way in which a hcp structure can transform into the fcc form is by shearing on close packed planes, the crystallographic orientation relationship being a habit plane of $(0002)_{\rm hcp}$ parallel to $\{111\}_{\rm fcc}$ with a $\langle 1010\rangle_{\rm hcp}$ direction parallel to a $\langle 112\rangle_{\rm fcc}$ direction. Underlying suggested theories of the transformation mechanism is a motion of a $6\langle 112\rangle$ partial dislocations across $\{111\}$ planes in the cubic lattice; the transformation shear on cooling is in a $\langle 112\rangle$ direction for Co-Ni alloy,[28] which undergoes the martensitic transition but at a lower temperature than in Co itself.[29] Displacive martensitic phase transitions of the elastic type, which tend to second-order character are normally associated with the long-wavelength acoustic mode softening; an example is the weakly first-order fcc to fct elastic phase transition in In-Tl alloys, which is also denoted as being martensitic, and for which freezing-in of a soft **N**[110] **U**[110] shear-mode displacement leads to the structural change.[30,31] However, the temperature dependence of the shear stiffness $(C_{11}-C_{12})/2$ of the $Co_{75}Mn_{25}$ alloy [Fig. 2(c)] does not evidence such acoustic mode softening. In fact for the $\varepsilon\rightarrow\gamma$ transition in Co and its alloys with Mn the point group of the product phase is not a subgroup of the parent phase: the driving mechanism cannot be acoustic shear-mode softening. Were there to be any shear-mode softening, then the corresponding elastic stiffness would be expected to change with temperature (or pressure) much more than the other tensor components. In the case of Co itself it was pointed out[32] that softening might happen much nearer the $\varepsilon\rightarrow\gamma$ transition than could be achieved experimentally; however, for the $Co_{75}Mn_{25}$ alloy the temperature (and pressure) effects obtained here in the vicinity of the transition show no evidence of mode softening effects: it is highly probable that this is also true for Co itself.

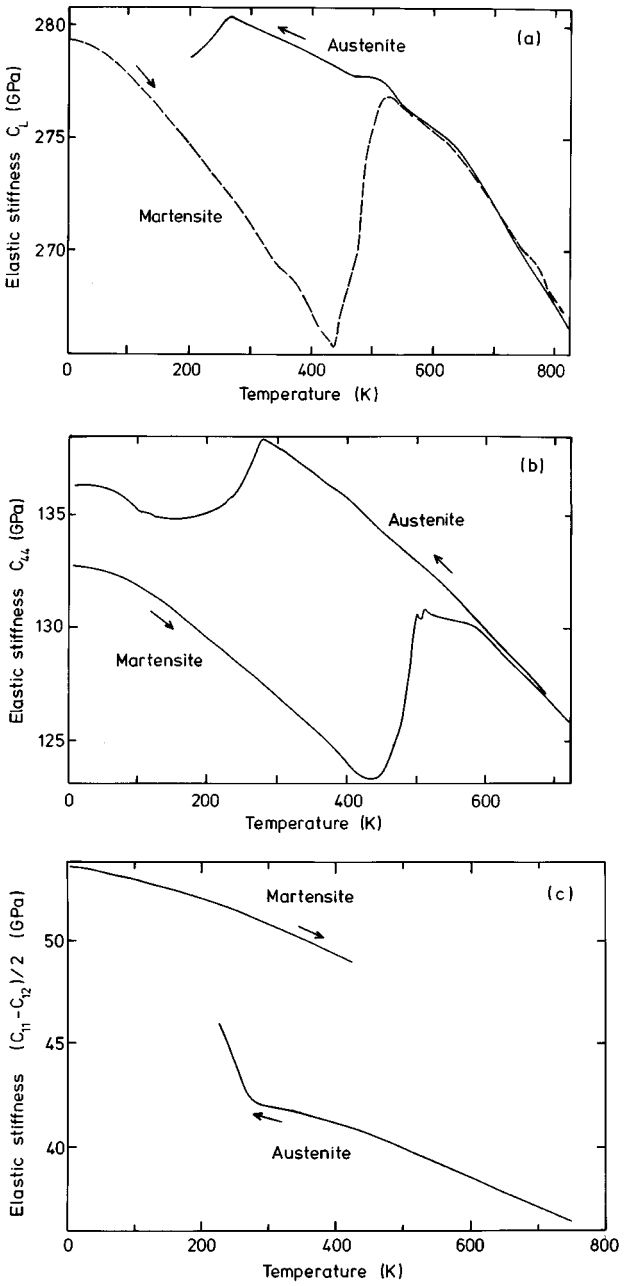

FIG. 2. The temperature dependences of the elastic stiffnesses of the (a) longitudinal C_L mode, (b) shear C_{44}, and (c) shear C' modes for the $Co_{75}Mn_{25}$ alloy which undergoes a strongly first order fcc (γ) to hcp (ε) martensitic transition. The pulse-echo-overlap method (Ref. 16) used to make these measurements is capable of resolution of velocity changes to 1 part in 10^5: the structure of the velocity-temperature dependence is reliable, while the absolute error corresponds to that quoted in Table I(a).

V. THE HYDROSTATIC PRESSURE DERIVATIVES OF THE ELASTIC STIFFNESS TENSOR COMPONENTS AND THE COMPRESSIONS OF Co-Mn AND OTHER INVARS

The pressure dependences of the ultrasonic wave velocities for the longitudinal C_L mode and the two shear C' and C_{44} modes have been measured at room temperature for each of the alloys. The velocities of all acoustic modes propagated in each alloy increase with pressure. The data are reproducible under pressure cycling and show no measurable hysteresis effects. The hydrostatic-pressure derivatives $(\partial C_{IJ}/\partial P)_{P=0}$ of C_{IJ} have been obtained from the ultrasonic measurements under pressure by using[18]

$$\left(\frac{\partial C_{IJ}}{\partial P}\right)_{P=0} = (C_{IJ})_{P=0}\left(\frac{2f'}{f_0} + \frac{1}{3B^T}\right)_{P=0}, \qquad (1)$$

where B^T is the isothermal bulk modulus, f_0 is the pulse-echo-overlap frequency at atmospheric pressure, and f' is its pressure derivative. The data for $(\partial C_{IJ}/\partial P)_{P=0}$ determined in the zero pressure limit [Table III(a)] establish trends that can be compared with those for other AFM and FM alloys [Table III(b)]. For the Co-Mn alloys each of the $(\partial C_{IJ}/\partial P)_{P=0}$ is positive, showing that the elastic stiffnesses and thus the slopes of the acoustic mode dispersion curves, at the long-wavelength limit, increase with pressure in the normal way. The application of pressure does not induce acoustic mode softening for any of these alloys. Most alloys follow the common trend for cubic crystals: $(\partial C_{11}/\partial P)_{P=0} > (\partial C_{44}/\partial P)_{P=0} > (\partial C'/\partial P)_{P=0}$. The derivative $(\partial C_{11}/\partial P)_{P=0}$ is the largest for most fcc materials because the higher-order elastic effects involved are dominated by nearest-neighbor repulsive forces. For the $Co_{46}Mn_{54}$ alloy $(\partial C_{11}/\partial P)_{P=0}$ and $(\partial C_{44}/\partial P)_{P=0}$ are the same within experimental error [Table III(a)].

As a consequence of the magnetovolume effect, in general, there is a close correlation between the magnitudes of the Invar anomaly in the thermal expansion and the pressure derivative of the elastic stiffness of the longitudinal acoustic mode and that of the bulk modulus (see, for instance Ref. 20). In the Invar region, the FM $Fe_{72}Pt_{28}$ alloy has large negative values of thermal expansion[33] and hydrostatic-pressure derivatives $(\partial C_{11}/\partial P)_{P=0}$ and $(\partial B^S/\partial P)_{P=0}$.[24,34] Analysis[35] of the magnetoelastic behavior in the vicinity of the FM transition using Landau theory has shown that the abrupt change in the bulk modulus[36] and the change incurred in $(\partial B^S/\partial P)_{P=0}$[24,34] at the transition can be interpreted quantitatively: magnetism governs the softening of $Fe_{72}Pt_{28}$ as it is lowered through its Curie temperature. In addition this phenomenological magnetoelasticity approach gives good agreement with the value of $(\partial B^S/\partial P)_{P=0}$ when $Fe_{72}Pt_{28}$ transforms from the paramagnetic to the ferromagnetic state, explaining the remarkable property of this Invar alloy of becoming more compressible as pressure is increased. In accord with this, in the case of the classic FM Invar material $Fe_{65}Ni_{35}$ there is a pause in the thermal expansion coupled with an almost zero value of $(\partial B^S/\partial P)_{P=0}$ in the same temperature interval.[34] The magnetoelastic effects in FM alloys, which produce magnetovolume instability, lead to softening of the long-wavelength acoustic modes and the consequent negative thermal expansion. Compared with that in FM alloys the magnetovolume instability in AFM alloys is much weaker:[20] The anomaly in the thermal expansion of $Co_{46}Mn_{54}$ (Ref. 11) is much less pronounced and $(\partial B^S/\partial P)_{P=0}$ is positive [Table III(a)].

There is often a marked difference in behavior between magnetic alloys, whose properties are influenced strongly by magnetovolume effects. This feature of transition-metal alloys and elements shows up in the volume compression

TABLE III. (a) Hydrostatic pressure derivatives $(\partial C_{IJ}/\partial P)_{P=0}$ of the elastic stiffness tensor components and $(\partial B^S/\partial P)_{P=0}$ of the adiabatic bulk modulus of fcc CoMn alloys. (b) Hydrostatic pressure derivatives $(\partial C_{IJ}/\partial P)_{P=0}$ of the elastic stiffness tensor components and $(\partial B^S/\partial P)_{P=0}$ of the adiabatic bulk modulus of transition-metal alloys at room temperature.

(a)

	$Co_{75}Mn_{25}$ (293 K) FM austenite phase	$Co_{68}Mn_{32}$ (293 K) paramagnetic		$Co_{52}Mn_{48}$ (291 K) AFM		$Co_{46}Mn_{54}$ (298 K) AFM	
		[110] mode	[001] mode	[110] mode	[001] mode	[110] mode	[001] mode
$(\partial C_{11}/\partial P)_{P=0}$	11.0±0.4	16.1±0.3	16.3±0.1	12.8±0.3	12.6±0.1	6.44±0.3	6.67±0.1
$(\partial C_{44}/\partial P)_{P=0}$	8.0±0.2	6.2±0.1	6.3±0.2	4.2±0.1	4.1±0.2	6.6±0.2	6.7±0.2
$(\partial C_{12}/\partial P)_{P=0}$	4.8±0.4	11.1±0.3		9.8±0.3		1.7±0.3	
$(\partial C'/\partial P)_{P=0}$	3.1±0.1	2.47±0.05		1.53±0.05		2.4±0.1	
$(\partial C_L/\partial P)_{P=0}$	15.9±0.3	19.8±0.3		15.5±0.3		10.6±0.2	
$(\partial B^S/\partial P)_{P=0}$	6.8±0.4	12.8±0.1		10.8±0.1		3.25±0.08	

(b)

	$Fe_{60}Mn_{40}$ (293 K) AFM	$Mn_{73}Ni_{27}$ (293 K) AFM	$Mn_{80.5}Ni_{19.5}$ (293 K) AFM	$Mn_{78}Pt_{22}$ (293 K) AFM	$Co_{68}Ni_{32}$ (295 K) FM	$Fe_{72}Pt_{28}$ (290 K) FM
Ref.	20	21	21	22	23	24
$(\partial C_{11}/\partial P)_{P=0}$	10.07±0.2	5.2	4.2	6.2±0.1	7.35	−19.2
$(\partial C_{12}/\partial P)_{P=0}$	7.15±0.21	3.2	3.8	4.2±0.3	6.39	−26.0
$(\partial C_{44}/\partial P)_{P=0}$	3.84±0.06	3.5	4.9	4.3±0.1	2.65	0.6
$(\partial C'/\partial P)_{P=0}$	1.46±0.05	0.9	0.2	1.0±0.1	0.48	3.4
$(\partial C_L/\partial P)_{P=0}$	12.45±0.2	7.7	8.9	9.5±0.2	9.52	−22.0
$(\partial B^S/\partial P)_{P=0}$	8.12±0.1	3.9	3.9	4.8±0.2	6.71	−23.7

$V(P)/V_0$ which can be obtained from measurements of the elastic stiffnesses and their hydrostatic-pressure dependences using an equation of state such as that of Murnaghan[37] which in logarithmic form is

$$\ln\left(\frac{V_0}{V(P)}\right)=\frac{1}{B_0'^T}\ln\left(\frac{B_0'^T}{B_0^T}P+1\right), \tag{2}$$

where B_0^T and $B_0'^T$ are the isothermal bulk modulus and its pressure derivative at zero pressure respectively. Inspection of the data for B_0^T [Table I(a)] and $(\partial B^S/\partial P)_{P=0}$ [Table III(a)] indicates that due to the magnetovolume effects the compression of AFM alloys is much enhanced compared with transition metals and alloys in which such effects are absent.

VI. GRÜNEISEN PARAMETERS AND ACOUSTIC MODE VIBRATIONAL ANHARMONICITY OF AFM $Co_{46}Mn_{54}$

It is useful to discuss the vibrational anharmonicity in terms of Grüneisen parameters, which quantify the volume or strain dependence of the lattice vibrational frequencies. The mode Grüneisen parameters $\gamma(p,N)$ for the antiferromagnetic $Co_{46}Mn_{54}$ alloy, calculated following the method introduced by Brugger and Fritz[38] (see also, Refs. 20 and 22), are given as a function of wave propagation direction in Fig. 3. The Grüneisen parameters for the longitudinal modes are almost independent of propagation direction. An unusual feature is that the longitudinal mode Grüneisen parameters are smaller than those for shear modes: at the zone center the longitudinal-mode acoustic phonons are softer than those of the shear modes. This is a reflection of stronger magnetovolume interaction with longitudinal than with shear modes. However, the longitudinal modes $\gamma(p,N)$ are not so strikingly anomalous in the AFM alloys as they are in FM Invars for which the magnetovolume interaction is much stronger. For example for $Fe_{72}Pt_{28}$, in the temperature range between about 260 and 390 K, the long-wavelength longitudinal acoustic mode $\gamma(p,N)$ is negative[24,34] accounting for its negative thermal expansion in this temperature range:[33] soft longitudinal acoustic modes play an important role in the Invar behavior of ferromagnetic $Fe_{72}Pt_{28}$.

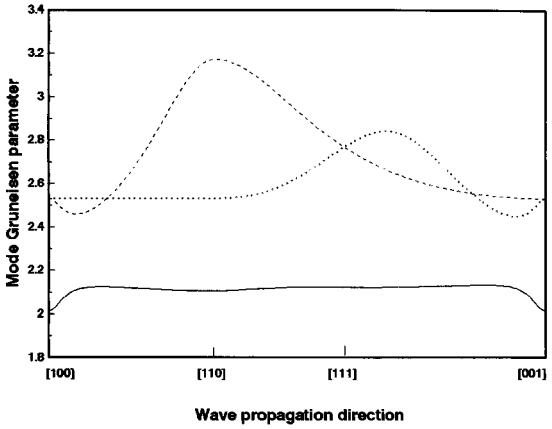

FIG. 3. Long-wavelength longitudinal (solid line) and shear (dashed and dotted lines) acoustic-mode Grüneisen parameters of $Co_{46}Mn_{54}$ as a function of mode propagation direction at 298 K.

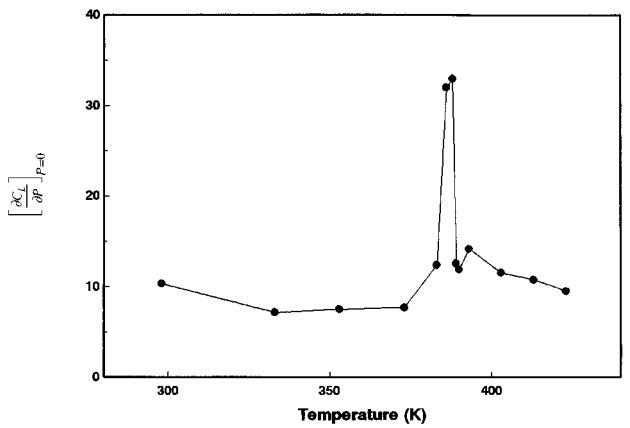

FIG. 4. The temperature dependence of the hydrostatic-pressure derivative $(\partial C_L/\partial P)_{P=0}$ for the $Co_{46}Mn_{54}$ alloy determined from measurements made on the longitudinal acoustic wave mode propagated along the [110] direction.

The thermal expansion includes contributions from phonons of wave vectors spanning the entire Brillouin zone in all branches. In the quasiharmonic approximation the thermal Grüneisen parameter γ^{th} is the weighted average of all the individual excited mode Grüneisen parameters $\gamma_i(=-\partial \ln \omega/\partial \ln V)$ and is given by

$$\gamma^{\text{th}}=\sum_i C_i\gamma_i \Big/ \sum_i C_i=\alpha VB^S/C_P=\alpha VB^T/C_V, \quad (3)$$

where C_i represents the Einstein heat capacity associated with a mode i and reflects the contribution of this mode to γ^{th}, V is the molar volume, α is the volume thermal expansion coefficient, C_P and C_V are specific heats at constant pressure and constant volume respectively. In the absence of specific-heat data, γ^{th} cannot be determined for Co-Mn alloys. However, the mean elastic Grüneisen parameter γ^{el}, which arises solely from the acoustic modes in the long-wavelength limit, can be obtained by the integration

$$\gamma^{\text{el}}=\frac{\sum_{p=1}^{3}\int_\Omega \gamma(p,N)d\Omega}{\sum_{p=1}^{3}\int_\Omega d\Omega}, \quad (4)$$

where the subscript Ω means integration over the whole solid angle. The values of γ^{el} obtained for $Co_{46}Mn_{54}$ and $Co_{68}Mn_{32}$ are compared with those of other transition-metal alloys in Table IV. In the case of the FM $Fe_{72}Pt_{28}$ alloy, the occurrence of negative longitudinal acoustic mode Grüneisen γ's leads to a negative γ^{el}—in accord with the negative thermal expansion of this Invar.

To establish how the effects of pressure on a longitudinal acoustic mode alter as the temperature is increased up to T_N, the hydrostatic-pressure derivative $(\partial C_L/\partial P)_{P=0}$ has been determined for the $Co_{46}Mn_{54}$ alloy as a function of temperature. The data for $(\partial C_L/\partial P)_{P=0}$, plotted in Fig. 4, show a sharp peak at about 388 K, somewhat below T_N; the value of $(\partial C_L/\partial P)_{P=0}$ at this temperature is about three times as large as that at room temperature. The value of $(\partial C_L/\partial P)_{P=0}$ commences to rise sharply at about 380 K and falls quickly above 388 K. This behavior bears some resemblance to that found[21] previously for $Mn_{73}Ni_{27}$ for which both $(\partial C_{11}/\partial P)_{P=0}$ and $(\partial C_L/\partial P)_{P=0}$ were found to increase strongly with temperature in the AFM state and then decrease substantially near T_N: considerable changes in the interatomic repulsive forces and in the long-wavelength acoustic-phonon anharmonicities take place with AFM ordering. In $Co_{46}Mn_{54}$ the magnetoelastic interaction has its strongest effect on the nonlinear acoustic properties, associated with the longitudinal modes, about 37 K below the Néel temperature. The particularly large effects on $(\partial C_L/\partial P)_{P=0}$ around the Néel temperature can be linked directly to the strong magnetoelastic coupling to the long-wavelength longitudinal phonons, which produces the small values of C_L and C_{11} [Table I(a)]. By using the data obtained for $(\partial C_L/\partial P)_{P=0}$ of $Co_{46}Mn_{54}$ from 333 to 423 K (Fig. 4), the temperature dependence of the mode Grüneisen parameter $\gamma_{L[110]}$ of the longitudinal mode propagating along the [110] direction has been determined (Table V). It can be seen from the table that a maximum occurs at 388 K with a value of 7.0. The response of the phonon frequency of this mode to the pressure-induced change in the volume of the alloy is extremely large. The vibrational anharmonicity of the longi-

TABLE IV. The mean acoustic mode Grüneisen parameter γ^{el} of Co-Mn alloys and other 3*d* transition metal alloys at room temperature. For corresponding references see Table III(b).

$Co_{68}Mn_{32}$ (293 K) PM	$Co_{46}Mn_{54}$ (298 K) AFM	$Fe_{60}Mn_{40}$ (293 K) AFM	$Mn_{73}Ni_{27}$ (293 K) AFM	$Mn_{80.5}Ni_{19.5}$ (293 K) AFM	$Mn_{78}Pt_{22}$ (293 K) AFM	$Co_{68}Ni_{32}$ (295 K) FM	$Fe_{72}Pt_{28}$ (290 K) FM
3.52	2.50	2.12	1.59	1.12	1.35	2.04	−0.60

TABLE V. The dependence of the Grüneisen parameter $\gamma_{L[110]}$ of the longitudinal acoustic wave mode along the [110] direction for $Co_{46}Mn_{54}$ alloy upon temperature from 333 to 423 K.

T(K)	$\gamma_{L[110]}$	T(K)	$\gamma_{L[110]}$	T(K)	$\gamma_{L[110]}$
333	1.37	386	6.79	393	2.91
353	1.45	388	7.01	403	2.35
373	1.50	389	2.57	413	2.20
383	2.53	390	2.42	423	1.95

tudinal acoustic mode is markedly enhanced by the magnetovolume effects just below T_N.

VII. CONCLUSIONS

The velocities of the ultrasonic modes propagated along the [110] and [001] directions of single crystals of alloys with compositions $Co_{75}Mn_{25}$, $Co_{68}Mn_{32}$, $Co_{52}Mn_{48}$, and $Co_{46}Mn_{54}$ have been measured as functions of temperature and hydrostatic pressure. There are several interesting features to note, which shed light on the elastic and nonlinear acoustic and lattice dynamical properties of fcc Co-Mn alloys. They can be summarized as follows.

(i) The volume-dependent elastic stiffnesses C_{11} and C_L and the bulk modulus B^S of the Co-Mn alloys are small in comparison with those of $3d$ transition-metal elements.

(ii) The $Co_{68}Mn_{32}$ alloy does not undergo any transitions in the temperature range from 4.2 to about 750 K. Its elastic stiffnesses can be considered to be representative of the properties of the paramagnetic state of Co-Mn alloys.

(iii) The $Co_{52}Mn_{48}$ and $Co_{46}Mn_{54}$ alloys are in the AFM phase at room temperature. Their elastic-stiffness tensor components are affected by the onset of antiferromagnetic ordering and strong magnetoelastic coupling in the AFM phase. Softening of the bulk modulus takes place because of the appearance of a spontaneous volume strain at the Néel temperature.

(iv) The $Co_{75}Mn_{25}$ alloy falls in the FM phase region; the Curie temperature is about 634 K. This alloy undergoes $\varepsilon \rightarrow \gamma$ and $\gamma \rightarrow \varepsilon$ transitions, when its temperature is altered. On warming up the start temperature for the $\varepsilon \rightarrow \gamma$ transition is at about 436 K and completion temperature is at 528 K. On cooling the $\gamma \rightarrow \varepsilon$ transition commences at 272 K. This marked hysteresis effect shows that the $\varepsilon \rightarrow \gamma$ transition is strongly first order. As anticipated for this particular structural transformation in this alloy there is no pronounced acoustic mode softening. This is probably also true for the $\varepsilon \rightarrow \gamma$ transition in Co itself.

(v) For all the Co-Mn alloys studied the hydrostatic-pressure derivatives $(\partial C_{11}/\partial P)_{P=0}$ of the elastic stiffnesses and $(\partial B^S/\partial P)_{P=0}$ of the bulk modulus are positive. Application of pressure does not induce acoustic mode softening for any of these alloys.

(vi) The longitudinal mode Grüneisen parameters for the AFM $Co_{46}Mn_{54}$ alloy show the unusual feature of being smaller than those for shear modes: the zone-center longitudinal-mode acoustic phonons are softer than the shear phonons on account of a stronger magnetovolume interaction with longitudinal than with shear modes. The long-wavelength longitudinal acoustic mode Grüneisen parameter $\gamma_{L[110]}$ of this alloy passes through a maximum value of 7.0 at 388 K, just below the Néel temperature T_N: the vibrational anharmonicity of this mode is markedly enhanced by the magnetovolume effects in the AFM state.

ACKNOWLEDGMENTS

We are grateful to the Deutsche Forschungsgemeinschaft (FSB166) and NATO (Scientific and Environmental Affairs Division, Grant No. CRG960584) for financial support. We would also like to thank Dr. U. Kawald for valuable discussions and E. F. Lambson and Li Jiaqiang for technical assistance.

*Permanent address: Department of Physics, University of Cape Town, Rondebosch, 7700, South Africa.

†Permanent address: Hacettepe University, Department of Physics, Beytepe, 06532 Ankara, Turkey.

[1] E. F. Wassermann, Phys. Scr. **T25**, 209 (1989).

[2] E. F. Wassermann, M. Acet, and W. Pepperhoff, J. Magn. Magn. Mater. **90**&**91**, 126 (1990).

[3] V. L. Moruzzi, Physica B **161**, 99 (1989).

[4] E. F. Wassermann, Europhys. News **22**, 150 (1991).

[5] A. Z. Men'shikov, G. A. Takzei, Yu. A. Dorofeev, V. A. Kazantsev, A. K. Kostyshin, and I. I. Sych, Sov. Phys. JETP **62**, 734 (1985).

[6] M. Acet, C. John, and E. F. Wassermann, J. Appl. Phys. **70**, 6556 (1991).

[7] M. Matsui, T. Ido, K. Sato, and K. Adachi, J. Phys. Soc. Japan **28**, 791 (1970).

[8] K. Adachi, K. Sato, M. Matsui, and S. Mitani, J. Phys. Soc. Japan **35**, 426 (1973).

[9] E. F. Wassermann, in *Cooperative Dynamics in Complex Systems*, edited by H. Takayama, Springer Series in Synergetics Vol. 43 (Springer, Berlin, 1989).

[10] E. F. Wassermann, J. Magn. Magn. Mater. **100**, 346 (1991).

[11] C. John, H. Zähres, M. Acet, W. Stamm, E. F. Wassermann, and W. Pepperhoff, J. Appl. Phys. **67**, 5268 (1990).

[12] L. Néel, J. Phys. Soc. Jpn. **17**, 672 (1962).

[13] Q. A. Pankhurst and R. J. Pollard, J. Phys. Condens. Matter **5**, 8487 (1993).

[14] A. Z. Men'shikov and Yu. A. Dorofeev, JETP Lett. **40**, 791 (1984).

[15] U. Kawald, O. Mitze, H. Bach, J. Pelzl, and G. A. Saunders, J. Phys. Condens. Matter **6**, 9697 (1994).

[16] E. P. Papadakis, J. Acoust. Soc. Am. **42**, 1045 (1967).

[17] R. N. Thurston and K. Brugger, Phys. Rev. **133**, A1604 (1964).

[18] R. N. Thurston, Proc. IEEE **53**, 1320 (1965).

[19] R. F. S. Hearmon, in *Elastic, Piezoelectric, Pyroelectric Piezooptic, Electrooptic Constants and Nonlinear Dielectric Susceptibilities of Crystals*, edited by K.-H. Hellwege, Landolt-Bornstein, New Series, Group 3, Vol. 11, Part b (Springer-Verlag, Berlin, 1979).

[20] M. Cankurtaran, G. A. Saunders, P. Ray, Q. Wang, U. Kawald, J. Pelzl, and H. Bach, Phys. Rev. B **47**, 3161 (1993).

[21] G. A. Saunders and M. D. Salleh, Philos. Mag. B **68**, 437 (1993).

[22] G. A. Saunders, M. Cankurtaran, P. Ray, J. Pelzl, and H. Bach, Phys. Rev. B **48**, 3216 (1993).

[23] W. F. Weston and A. V. Granato, Phys. Rev. B **12**, 5355 (1975).

[24] Ll. Mañosa, G. A. Saunders, H. Radhi, U. Kawald, J. Pelzl, and

H. Bach, Phys. Rev. B. **45**, 2224 (1992).
[25] E. S. Fisher and D. Dever, Trans. Metal. Soc. AIME **239**, 48 (1967).
[26] J. T. Lenkkeri, J. Phys. F **11**, 1997 (1981).
[27] V. L. Moruzzi, Phys. Rev. B **41**, 6939 (1990).
[28] E. de Lamotte and C. Alstetter, Trans. Metal. Soc. AIME **245**, 651 (1969).
[29] J. B. Hess and C. S. Barrett, Trans. Metal. Soc. AIME **194**, 645 (1952).
[30] M. P. Brassington and G. A. Saunders, Phys. Rev. Lett. **48**, 159 (1982).
[31] G. A. Saunders, J. E. Macdonald, J. D. Comins, and E. A. Saunders, Phys. Rev. B. **34**, 2064 (1986).
[32] Y. K. Yogurtcu, G. A. Saunders, and P. C. Riedi, Philos. Mag. B **52**, 833 (1985).
[33] K. Sumiyama, M. Shiga, M. Morioka, and Y. Nakamura, J. Phys. F **9**, 1665 (1979).
[34] Ll. Mañosa, G. A. Saunders, H. Radhi, U. Kawald, J. Pelzl, and H. Bach, J. Phys. Condens. Matter **3**, 2273 (1991).
[35] D. Wagner, V. M. Zverev, V. P. Silin, and M. Thon, JETP Lett. **56**, 595 (1992).
[36] G. Hausch, J. Phys. Soc. Jpn. **37**, 819 (1974).
[37] F. D. Murnaghan, Proc. Natl. Acad. Sci. USA **30**, 244 (1944).
[38] K. Brugger and T. C. Fritz, Phys. Rev. **157**, 524 (1967).